Nonlinear terahertz metamaterials with active electrical control

G. R. Keiser, N. Karl, P. Q. Liu, C. Tulloss, H.-T. Chen, A. J. Taylor, I. Brener, J. L. Reno, and D. M. Mittleman

Citation: Appl. Phys. Lett. **111**, 121101 (2017); doi: 10.1063/1.4990671
View online: http://dx.doi.org/10.1063/1.4990671
View Table of Contents: http://aip.scitation.org/toc/apl/111/12
Published by the American Institute of Physics

Nonlinear terahertz metamaterials with active electrical control

G. R. Keiser,[1,2,a)] N. Karl,[1] P. Q. Liu,[3,4,b)] C. Tulloss,[1] H.-T. Chen,[5] A. J. Taylor,[5] I. Brener,[3] J. L. Reno,[3] and D. M. Mittleman[1,c)]
[1]*School of Engineering, Brown University, Providence, Rhode Island 02912, USA*
[2]*Department of Physics, Washington College, Chestertown, Maryland 21620, USA*
[3]*Center for Integrated Nanotechnologies, Sandia National Laboratories, Albuquerque, New Mexico 87185, USA*
[4]*Department of Electrical Engineering, University at Buffalo, Buffalo, New York 14260, USA*
[5]*Center for Integrated Nanotechnologies, Los Alamos National Laboratory, Los Alamos, New Mexico 87545, USA*

(Received 16 June 2017; accepted 5 September 2017; published online 19 September 2017)

We present a study of an electrically modulated nonlinear metamaterial consisting of an array of split-ring resonators fabricated on n-type gallium arsenide. The resonant metamaterial nonlinearity appears as an intensity-dependent transmission minimum at terahertz frequencies and arises from the interaction between local electric fields in the split-ring resonator (SRR) capacitive gaps and charge carriers in the n-type substrate. We investigate the active tuning range of the metamaterial device as the incident terahertz field intensity is increased and conversely the effect of an applied DC bias on the terahertz field-induced nonlinear modulation of the metamaterial response. Applying a DC bias to the metamaterial sample alters the nonlinear response and reduces the net nonlinear modulation. Similarly, increasing the incident terahertz field intensity decreases the net modulation induced by an applied DC bias. We interpret these results in terms of DC and terahertz-field-assisted carrier acceleration, scattering, and multiplication processes, highlighting the unique nature of this DC-field modulated terahertz nonlinearity. *Published by AIP Publishing.*
[http://dx.doi.org/10.1063/1.4990671]

At terahertz (THz) frequencies, metamaterials (MMs) have become a popular platform for engineering new components and capabilities.[1] MM strategies have proven to be effective for engineering passive optical devices across the electromagnetic spectrum, including negative index materials,[2] microwave cloaks,[3] perfect absorbers,[4,5] and memory materials.[6] It is also possible to implement electrical and optical control of MMs via active circuit elements,[7] electrically or optically active substrates,[8,9] or structural MEMS actuation,[10] allowing for active MM components for use as THz thermal detectors,[11] diffraction modulators,[12] spatial light modulators,[13] and tunable filters[14] to name just a few examples.

More recently, MMs have been used to design enhanced optical nonlinearities through the combination of subwavelength nonlinear elements and resonant electric field enhancement. At microwave frequencies and below, split-ring resonators (SRRs) combined with diodes and varactors have produced nonlinear MMs for second harmonic generation,[15] wave mixing,[16] and nonlinear beam shaping.[17] At THz frequencies, lumped circuit elements are generally too large to be included within the SRR elements. Instead, one can use the local electric field enhancement within the SRR capacitive gap[18] to couple to resonant nonlinearities in an underlying substrate material. This results in amplified nonlinearities that manifest in the MM's electromagnetic response. Semiconductor substrates,[19,20] superconducting films,[21–23] and transition metal oxides[24] have all been used to effectively produce enhanced THz nonlinear optics, including saturable absorbers[25,26] and THz second harmonic generation.[27]

While much progress has been made in both active MM devices and nonlinear MMs, a MM with an actively tunable nonlinear optical response is yet to be realized experimentally. In this letter, we present the design, fabrication, and characterization of such an electrically tunable nonlinear MM for THz frequencies. Our device consists of a planar array of SRRs fabricated on an n-type gallium arsenide (n-GaAs) layer grown on a semi-insulating GaAs (SI-GaAs) substrate. A DC voltage bias can be applied to actively control the carrier density within the n-GaAs layer. The resonant nonlinear response appears as an intensity-dependent transmission arising from the interaction between local electric fields in the SRR capacitive gap and charge carriers in the n-GaAs layer. We compare the modulation depth in the MM response induced via the applied DC bias with the nonlinear modulation induced by the intense THz fields. We also show that applying a DC bias to the MM sample alters the nonlinear response of the device, reducing the net nonlinear modulation by $\sim$2 dB. Finally, we characterize the active modulation range of the MM and how it changes as the strength of the THz excitation source increases.

Figure 1 shows a representative micrograph of the two-dimensional MM along with a schematic of the unit cell. The SRR has a polarization insensitive 4-fold symmetric design with capacitive gaps on the sides of the structure. The dimensions are chosen such that the SRR resonance falls at 0.4 THz, near the peak of our experimental THz spectrum. The length of the SRR is $L = 66\ \mu$m, unit cell periodicity $P = 88\ \mu$m, linewidth $w = 6\ \mu$m, and capacitive gap $g = 1\ \mu$m. The gold bars extending from the bottom end of the SRR join the resonators and connect with an electrode (not shown). The gold SRR array and the underlying n-GaAs layer form a Schottky junction, where a voltage bias can be

a)Experiment performed while author was at Brown University.
b)Experiment performed while author was at Sandia National Lab.
c)Author to whom correspondence should be addressed: daniel_mittleman@brown.edu

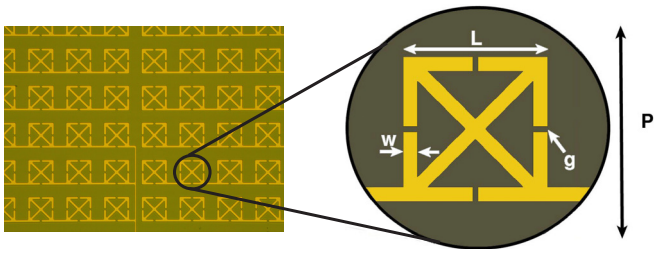

FIG. 1. Representative mircrograph of the two-dimensional MM structure and schematic of the SRR unit cell with relevant dimensions. L = 66 μm, P = 88 μm, w = 6 μm, and g = 1 μm.

applied between the Schottky contact and an ohmic contact on the GaAs substrate.[8] For this device, the n-GaAs layer has a doping density of $2 \times 10^{16}\,\mathrm{cm}^{-3}$ and a thickness $t = 1\,\mu$m, while the SI-GaAs substrate is $\sim$500 μm thick.

Electrical tuning of the MM resonance is implemented by applying a DC voltage bias to deplete charge carriers in the n-GaAs layer in the region near the split gaps.[8] The nonlinear response of the MM arises from two separate effects. At lower THz fields around 40 kV/cm, intervalley scattering is induced by the interaction of charge carriers with the *incident* THz field and lowers the carrier mobility.[19,28] At higher field strengths >100 kV/cm, impact ionization results from the interaction of charge carriers with the enhanced *resonant* THz fields localized in the MM capacitive gap, which increases the in-gap GaAs conductivity.[19]

Figure 2 shows numerical simulations of how these two processes change the MM response, using a commercial finite difference time domain solver. The conductivity of the n-GaAs epilayer is modeled using the known carrier concentration and a frequency independent mobility

$$\sigma = ne\mu, \tag{1}$$

where $n = 2 \times 10^{16}\,\mathrm{cm}^{-3}$ and e is the charge of an electron. The assumption of a frequency independent mobility is reasonable given the frequency range considered in this study (0.1 THz–0.8 THz). Figure 2(a) shows the effect of intervalley scattering on the MM transmission spectra. The scattering of carriers to satellite valleys in the GaAs band diagram, where the overall mobility of the carriers is lower due to a larger effective mass, effectively lowers the conductivity of the n-doped layer. This decreases the loss in the SRR and thus increases the resonance strength. We model intervalley scattering in simulation by directly lowering the carrier mobility. As the carrier mobility, μ, decreases uniformly across the n-GaAs film, the loss in the MM decreases, resulting in a stronger inductive-capacitive (LC) resonance. Figure 2(b) illustrates the opposite effect of impact ionization in the gap regions at higher THz field excitation. To simulate the confined, resonant nature of the impact ionization, the conductivity in the gap regions of n-GaAs, σ_g, is increased, while the mobility of n-GaAs away from the split gaps is held constant at 400 cm^2/Vs. As σ_g increases, current begins to pass through the capacitive gap regions, and the resistive loss in the SRRs increases. Thus, the resonance becomes weaker with increasing σ_g. We show below that the addition of the applied DC bias to our MM sample allows for tuning the MM resonance strength through the control of both the charge carrier density[8] and the field dependent carrier dynamics of the n-GaAs layer, i.e., by lowering the THz field threshold for impact ionization. The values of μ and σ_g used in these simulations were chosen to correspond to values considered in previous work on similar samples,[19] and the resulting simulated spectra corresponded well to our experimental data discussed below.

To characterize the MM's nonlinear response at varying values of applied bias, THz pulses with field strengths between 30 and 120 kV/cm were generated using the tilted-pulse-front technique in $LiNbO_3$ and focused onto the MM at normal incidence.[29,30] The THz field strength in our system was computed using the pulse energy, U (measured using a THz pyroelectric detector), the cross-sectional area of the terahertz spot at the sample position, A (measured with a THz camera), and the FWHM of the temporal envelope of the THz pulse, t. The pulse energy density and thus the THz electric field strength, E_{Thz}, can be calculated from this information, giving

$$E_{THz} = \sqrt{\frac{2U}{\epsilon_0 cAt}}. \tag{2}$$

where ϵ_0 is the permittivity of free space and c the speed of light in vacuum. More details on computing accurate values for A and t can be found in Ref. 31.

The incident THz fields excite the MM resonance, and the transmitted pulses are then measured using THz time-domain spectroscopy (THz-TDS). To measure the low field (linear) response, a commercial THz-TDS system was used. The THz transmission spectra were obtained through Fourier transform and normalized to a bare substrate.

Figure 3(a) shows the MM transmission response at low field THz excitation with increasing DC bias. This serves as

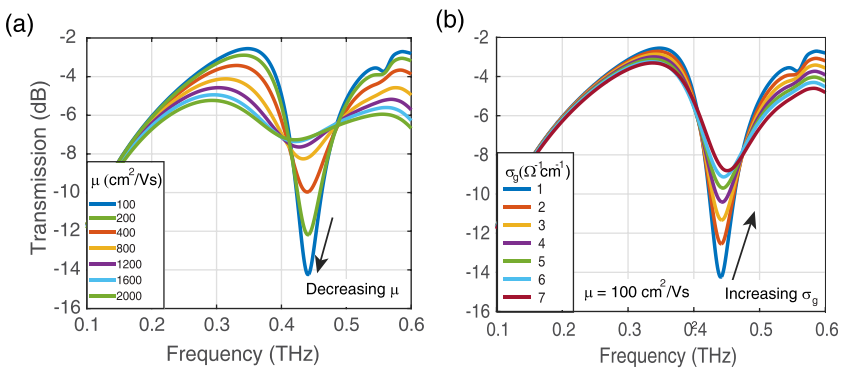

FIG. 2. Simulations of the MM transmission spectra. (a) Transmission spectra at various n-GaAs carrier mobilities, μ. (b) Transmission spectra for various capacitive gap conductivities, σ_g, while leaving μ constant.

a baseline check of the MM active response. Increasing the applied bias from 0 V to 15 V decreases the resonance depth by ∼4 dB due to carrier depletion in the substrate. The maximum carrier depletion is reached at 15 V, resulting in a resonance depth of ∼ −8 dB. The resonance saturates at this point, and further increasing the applied bias does not affect the response.

For comparison, Fig. 3(b) shows the MM's nonlinear, THz field-dependent response, while the applied DC bias is held constant at 0 V. Overall, there is good correspondence between our simulations and the experimental results of Fig. 3(b). The resonance frequency and maximum resonance depth overlap quite closely. The width of the resonance in the experiment is slightly larger than in simulation, but this is due to the limited frequency resolution of our experimental system.

In contrast to the DC induced modulation, increasing the incident THz fields from low field values to ∼50 kV/cm induces a transmission minimum of ∼ −13 dB, i.e., a total modulation of 9 dB. Further increasing the incident THz field induces impact ionization near the regions of field enhancement in the SRR capacitive gaps. The carrier concentration and thus the conductivity of the nGaAs layer increase, increasing the loss in the SRR and causing the resonance to become weaker. This results in a transmission minimum of ∼ −9 dB for 120 kV/cm THz excitation.

In brief, using high field THz pulses instead of a DC bias to modulate the resonance increases the modulation depth by about 5 dB. The larger modulation is a result of the local electric fields excited in the MM by the incident THz pulse. Figures 3(c) and 3(d) compare the simulated electric field magnitude in the MM unit cell for the cases of an applied 15 V DC bias and a 50 kV/cm THz excitation, respectively. Outside the capacitive gap regions, the electric fields induced by the applied bias and THz excitation are comparable in magnitude. However, the DC bias fields are largely confined to the regions around the SRR, while the THz fields extend throughout the MM unit cell. Thus, the DC bias depletes the carrier concentration near the SRR, and the resonance strength cannot increase further once all the carriers in this region are depleted.

In contrast, the extent of the THz fields simulated in Fig. 3(d) and the off-resonance, transmission modulation between the low field and 30 kV/cm spectra in Fig. 3(b) suggest that the THz fields interact with carriers both in regions near the SRR gaps and further away from the resonator. This interpretation is also consistent with results shown in previous work.[19] Due to intervalley scattering, the THz fields lower the carrier mobility across a percentage of the unit cell that is much larger than the region of carrier depletion induced by the DC bias. This results in a stronger resonance for THz excitation compared to the DC bias case and thus a larger modulation depth. Another observation is that increasing the DC bias also strengthens the resonance under THz excitation at 30 kV/cm, with resonant transmission minimum decreasing from ∼ −13 dB at 0 V bias shown in Fig. 3(b) to ∼ −15 dB at 15 V bias shown in Fig. 4(d), a change of about 2 dB. However, the corresponding net modulation depth, defined as the difference in transmission minimum between the low field and 30 kV/cm THz excitations, is reduced from ∼9 dB at 0 V bias to ∼7 dB at 15 V bias. This decrease is due to the larger resonance strength at low field excitation induced by the DC voltage bias, as shown in Fig. 4. This tunable nonlinear modulation is the result of the carrier depletion induced by the DC bias, leaving fewer carriers near the split-gaps to interact with the THz field and lowering the net nonlinear modulation, defined as the modulation in the resonance depth between the low-field and 30 kV/cm curves.

We also expect that the applied DC bias affects the charge carrier dynamics in the MM structure by lowering the threshold THz field required to induce impact ionization.

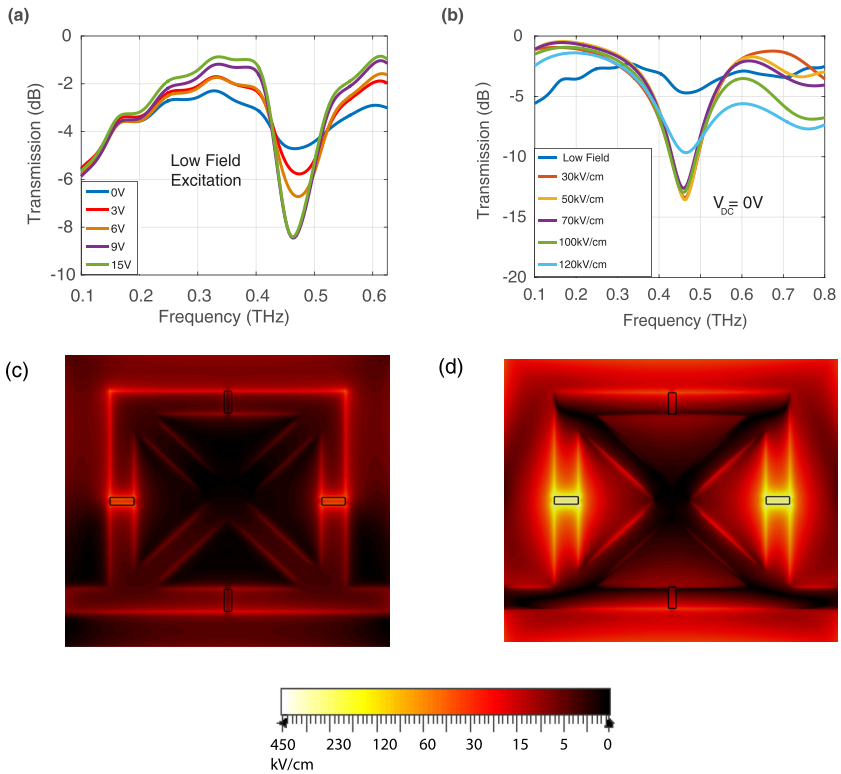

FIG. 3. (a) MM transmission spectra for different applied DC biases with a constant low field THz excitation. (b) MM transmission spectra for varying incident THz field strengths and a constant applied bias of 0 V. (c) Simulated electric field magnitude in the MM unit cell with a 15 V applied DC bias. (d) Simulated electric field magnitude in the MM unit cell under excitation with a 50 kV/cm THz pulse. DC bias fields are confined to the regions around the SRR, while the THz fields extend throughout the MM unit cell. Thus, the DC bias depletes the carrier concentration near the SRR, but the THz excitation lowers the carrier mobility across a larger percentage of the unit cell. This results in a stronger resonance compared to the DC bias case and thus a larger modulation depth.

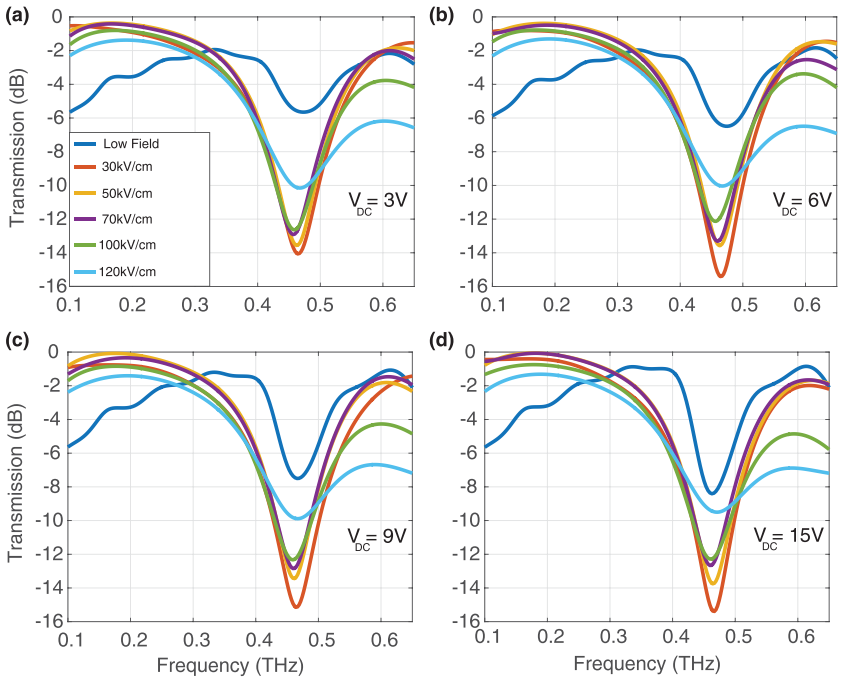

FIG. 4. Field dependence of the nonlinear MM transmission at applied biases of (a) 3 V, (b) 6 V, (c) 9 V, and (d) 15 V.

Our data in Fig. 4 are consistent with this interpretation. For 0 V applied bias, the resonance strength shown in Fig. 3(b) remains fairly constant between 30 kV/cm and 100 kV/cm THz field excitation. The resonance strength decreases only at the highest field value of 120 kV/cm where impact ionization is the dominant effect in the carrier dynamics. In contrast, for 3 and 6 V applied biases, shown in Figs. 4(a) and 4(b), 30 kV/cm THz field excitation strengthens the resonance and lowers the transmission minimum to −14 dB, which remains fairly constant until the field reaches 66 kV/cm, when it increases by ∼1 dB, suggesting the onset of impact ionization at lower fields. With 9 and 15 V applied biases shown in Figs. 4(c) and 4(d), the decrease in resonance strength induced by impact ionization is apparent for a THz field of 50 kV/cm or higher.

These results highlight the importance of considering nonlinear effects in MM designs for high field applications. Figure 5 summarizes the on-resonance transmission vs. incident THz field for varying applied DC biases. At low fields, the electrical modulation depth is the greatest, close to 4 dB, although the resonance strength is at its weakest. As the THz field is increased to 30 kV/cm, inter-valley scattering lowers the carrier mobility and increases the resonance strength, lowering the resonance minimum by ∼10 dB. Importantly, the electrical modulation range is also decreased to ∼2 dB. Further increasing the THz field intensity beyond this point results in an upward trend in the resonance minimum as impact ionization increases the charge carrier density and the loss in the MM resonators. At fields higher than 30 kV/cm, the electrical modulation depth drops to 1 dB or less, showing that the effectiveness of common active tuning schemes[8] can vary significantly depending on the intensity of the THz field excitation.

Finally, Fig. 5 also highlights the effect of the applied bias on impact ionization in the n-GaAs epilayer. For THz fields below 50 kV/cm, increasing the applied bias makes the resonance stronger and thus lowers the transmission minimum. However, for 100 kV/cm fields, this trend reverses. Although it is a small effect, increasing the applied bias on the MM for 100 kV/cm excitation causes the resonance minimum to increase rather than decrease, suggesting a weakened resonance. This small but repeatable effect most likely occurs because the addition of the strong local DC field in the gaps increases the probability for THz-field-induced impact ionization in these regions. We note that the DC bias is applied across the depletion region within the 1 μm thick n-GaAs epilayer. This results in a local DC electric field on the order of 150 kV/cm in the gap region of the MM, which is comparable in strength to the peak field of the incident THz radiation (although THz fields are further enhanced by the metamaterial resonance). As outlined in Fig. 6, the DC and THz fields overlap within the depletion region, as they both are perpendicular to the metal surface within its vicinity. Therefore, it is not surprising that the DC field constructively superimposes with THz field and can alter the nonlinear response of the n-GaAs epilayer to the incident intense THz field.

In conclusion, we fabricated and characterized an electrically active nonlinear MM for THz frequency applications. A DC bias can be applied to actively control both the resonance strength and its nonlinearity, via carrier depletion. The

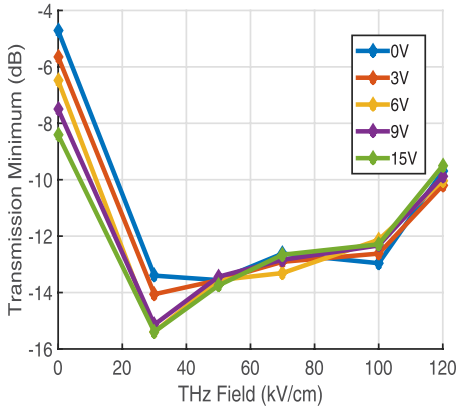

FIG. 5. Transmission minimum vs. incident THz field intensity at different applied DC biases.

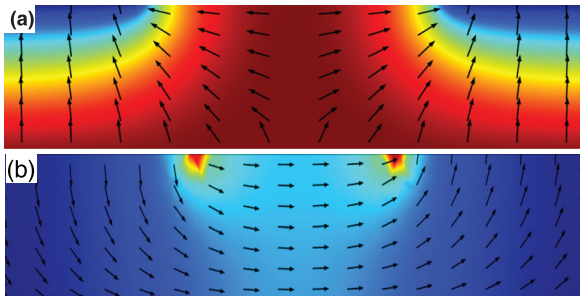

FIG. 6. (a) Cross-sectional plot of the simulated electric potential (arb. units) in the capacitive gap regions of the SRR due to the applied DC bias. The red color indicates higher potential. Arrows show the corresponding electric field direction. (b) Cross-sectional plot of the simulated resonant electric field magnitude (arb. units) due to THz excitation in the capacitive gap regions. The red color indicates higher electric field magnitude. Arrows indicate the direction of the THz electric field. In the vicinity of the capacitive gap (center of the above plots), the DC and THz electric fields are largely parallel and can add constructively.

resonant nonlinearity appears as an intensity-dependent transmission arising from THz induced intervalley carrier scattering and carrier dynamics in the n-GaAs layer. We compared the modulation depth in the MM response induced via the applied DC bias with the nonlinear modulation induced by the incident intense THz fields. We also show that applying a DC bias to the MM sample reduces the nonlinear modulation depth by $\sim$2 dB. Finally, we showed that the electrically active modulation depth of the MM decreases as the THz field intensity is increased. Our work provides an understanding of how the tunability of electrically active MMs changes for higher intensity THz excitation and also serves as a proof of principle for electrically active nonlinear THz devices.

We are grateful for support from the Army Research Office and the National Science Foundation for this project. This work was performed, in part, at the Center for Integrated Nanotechnologies, an Office of Science User Facility operated for the U.S. Department of Energy (DOE) Office of Science by Los Alamos National Laboratory (Contract No. DE-AC52-06NA25396) and Sandia National Laboratories (Contract No. DE-NA-0003525).

[1]P. W. Gwyn, "Filling the THz gap—high power sources and applications," Rep. Prog. Phys. **69**, 301 (2006).
[2]D. R. Smith, W. J. Padilla, D. C. Vier, S. C. Nemat-Nasser, and S. Schultz, "Composite medium with simultaneously negative permeability and permittivity," Phys. Rev. Lett. **84**, 4184 (2000).
[3]D. Schurig, J. J. Mock, B. J. Justice, S. A. Cummer, J. B. Pendry, A. F. Starr, and D. R. Smith, "Metamaterial electromagnetic cloak at microwave frequencies," Science **314**, 977 (2006).
[4]N. I. Landy, S. Sajuyigbe, J. J. Mock, D. R. Smith, and W. J. Padilla, "Perfect metamaterial absorber," Phys. Rev. Lett. **100**, 207402 (2008).
[5]H. Tao, N. I. Landy, C. M. Bingham, X. Zhang, R. D. Averitt, and W. J. Padilla, "A metamaterial absorber for the terahertz regime: Design, fabrication and characterization," Opt. Express **16**, 7181 (2008).
[6]T. Driscoll, H.-T. Kim, B.-G. Chae, B.-J. Kim, Y.-W. Lee, N. M. Jokerst, S. Palit, D. R. Smith, M. Di Ventra, and D. N. Basov, "Memory metamaterials," Science **325**, 1518 (2009).
[7]I. Gil, J. Bonache, J. Garcia-Garcia, and F. Martin, "Tunable metamaterial transmission lines based on varactor-loaded split-ring resonators," IEEE Trans. Microwave Theory Tech. **54**, 2665 (2006).
[8]H.-T. Chen, W. J. Padilla, J. M. O. Zide, A. C. Gossard, A. J. Taylor, and R. D. Averitt, "Active terahertz metamaterial devices," Nature **444**, 597 (2006).
[9]H. R. Seren, G. R. Keiser, L. Cao, J. Zhang, A. C. Strikwerda, K. Fan, G. D. Metcalfe, M. Wraback, X. Zhang, and R. D. Averitt, "Optically modulated multiband terahertz perfect absorber," Adv. Opt. Mater. **2**, 1221 (2014).
[10]X. Zhao, K. Fan, J. Zhang, G. R. Keiser, G. Duan, R. D. Averitt, and X. Zhang, "Voltage-tunable dual-layer terahertz metamaterials," Microsyst. Nanoeng. **2**, 16025 (2016).
[11]H. Tao, E. A. Kadlec, A. C. Strikwerda, K. Fan, W. J. Padilla, R. D. Averitt, E. A. Shaner, and X. Zhang, "Microwave and terahertz wave sensing with metamaterials," Opt. Express **19**, 21620 (2011).
[12]N. Karl, K. Reichel, H.-T. Chen, A. J. Taylor, I. Brener, A. Benz, J. L. Reno, R. Mendis, and D. M. Mittleman, "An electrically driven terahertz metamaterial diffractive modulator with more than 20 dB of dynamic range," Appl. Phys. Lett. **104**, 091115 (2014).
[13]W. L. Chan, H.-T. Chen, A. J. Taylor, I. Brener, M. J. Cich, and D. M. Mittleman, "A spatial light modulator for terahertz beams," Appl. Phys. Lett. **94**, 213511 (2009).
[14]I. Gil, J. Garcia-Garcia, J. Bonache, F. Martin, M. Sorolla, and R. Marques, "Varactor-loaded split ring resonators for tunable notch filters at microwave frequencies," Electron. Lett. **40**, 1347 (2004).
[15]A. Rose, D. Huang, and D. R. Smith, "Controlling the second harmonic in a phase-matched negative-index metamaterial," Phys. Rev. Lett. **107**, 063902 (2011).
[16]A. Rose, D. Huang, and D. R. Smith, "Nonlinear interference and unidirectional wave mixing in metamaterials," Phys. Rev. Lett. **110**, 063901 (2013).
[17]S. Keren-Zur, O. Avayu, L. Michaeli, and T. Ellenbogen, "Nonlinear beam shaping with plasmonic metasurfaces," ACS Photonics **3**, 117 (2016).
[18]G. R. Keiser, H. R. Seren, A. C. Strikwerda, X. Zhang, and R. D. Averitt, "Structural control of metamaterial oscillator strength and electric field enhancement at terahertz frequencies," Appl. Phys. Lett. **105**, 081112 (2014).
[19]K. Fan, H. Y. Hwang, M. Liu, A. C. Strikwerda, A. Sternbach, J. Zhang, X. Zhao, X. Zhang, K. A. Nelson, and R. D. Averitt, "Nonlinear terahertz metamaterials via field-enhanced carrier dynamics in GaAs," Phys. Rev. Lett. **110**, 217404 (2013).
[20]H. R. Seren, J. Zhang, G. R. Keiser, S. J. Maddox, X. Zhao, K. Fan, S. R. Bank, X. Zhang, and R. D. Averitt, "Nonlinear terahertz devices utilizing semiconducting plasmonic metamaterials," Light Sci. Appl. **5**, e16078 (2016).
[21]M. Ricci, N. Orloff, and S. M. Anlage, "Superconducting metamaterials," Appl. Phys. Lett. **87**, 034102 (2005).
[22]K. G. Nathaniel, G. P. Bradford, Jr., Y. H. Harold, C. B. Nathaniel, T. Darius, S. Ranjan, Y. Li, T. Daniel, A. T. Stuart, Q. X. Jia, J. T. Antoinette, A. N. Keith, and C. Hou-Tong, "Nonlinear high-temperature superconducting terahertz metamaterials," New J. Phys. **15**, 105016 (2013).
[23]C. Zhang, B. Jin, J. Han, I. Kawayama, H. Murakami, J. Wu, L. Kang, J. Chen, P. Wu, and M. Tonouchi, "Terahertz nonlinear superconducting metamaterials," Appl. Phys. Lett. **102**, 081121 (2013).
[24]M. Liu, H. Y. Hwang, H. Tao, A. C. Strikwerda, K. Fan, G. R. Keiser, A. J. Sternbach, K. G. West, S. Kittiwatanakul, J. Lu, S. A. Wolf, F. G. Omenetto, X. Zhang, K. A. Nelson, and R. D. Averitt, "Terahertz-field-induced insulator-to-metal transition in vanadium dioxide metamaterial," Nature **487**, 345 (2012).
[25]G. R. Keiser, J. Zhang, X. Zhao, X. Zhang, and R. D. Averitt, "Terahertz saturable absorption in superconducting metamaterials," J. Opt. Soc. Am. B **33**, 2649 (2016).
[26]X. Zhao, J. Zhang, K. Fan, G. Duan, G. D. Metcalfe, M. Wraback, X. Zhang, and R. D. Averitt, "Nonlinear terahertz metamaterial perfect absorbers using GaAs [Invited]," Photonics Res. **4**, A16–A21 (2016).
[27]H. Merbold, A. Bitzer, and T. Feurer, "Second harmonic generation based on strong field enhancement in nanostructured THz materials," Opt. Express **19**, 7262 (2011).
[28]F. Blanchard, L. Razzari, F. H. Su, G. Sharma, R. Morandotti, T. Ozaki, M. Reid, and F. A. Hegmann, "The dawn of ultrafast nonlinear optics in the terahertz regime," in *Nonlinear Photonics and Novel Optical Phenomena*, edited by Z. Chen and R. Morandotti (Springer, New York, 2012), pp. 297–323.
[29]K. Yeh, M. Hoffmann, J. Hebling, and K. A. Nelson, "Generation of 10 J ultrashort terahertz pulses by optical rectification," Appl. Phys. Lett. **90**, 171121 (2007).
[30]H. Hirori, A. Doi, F. Blanchard, and K. Tanaka, "Single-cycle terahertz pulses with amplitudes exceeding 1 MV/cm generated by optical rectification in LiNbO3," Appl. Phys. Lett. **98**, 091106 (2011).
[31]M. Clerici, M. Peccianti, B. E. Schmidt, L. Caspani, M. Shalaby, M. Giguere, A. Lotti, A. Couairon, F. Legare, T. Ozaki, D. Faccio, and R. Morandotti, "Wavelength scaling of terahertz generation by gas ionization," Phys. Rev. Lett. **110**, 253901 (2013).